Journal of Power Sources 224 (2013) 195–201

Contents lists available at SciVerse ScienceDirect

Journal of Power Sources

journal homepage: www.elsevier.com/locate/jpowsour

Composite material for supercapacitors formed by polymerization of aniline in the presence of graphene oxide nanosheets

Y.M. Shulga [a,*], S.A. Baskakov [a], V.V. Abalyaeva [a], O.N. Efimov [a], N.Y. Shulga [b], A. Michtchenko [c], L. Lartundo-Rojas [c], L.A. Moreno-R [c], J.G. Cabañas-Moreno [c], V.N. Vasilets [d]

[a] Institute of Problems of Chemical Physics, Russian Academy of Sciences, 142432 Chernogolovka, Moscow Region, Russia
[b] Moscow Steel and Alloys Institute, 117936 Moscow, Leninsky pr. 4, Russia
[c] Instituto Politecnico Nacional, CNMN, UPALM, 07738 Mexico City, DF, Mexico
[d] Institute for Energy Problems of Chemical Physics (Branch), Russian Academy of Sciences, 142432 Prosp. Acad. Semenova 2/10, Chernogolovka, Moscow Region, Russia

H I G H L I G H T S

► The composites of polyaniline with graphene oxide were analyzed.
► The graphene oxide is reduced partially in the process of polymerization.
► The specific capacitance of the composite in 1 M H_2SO_4 was found to be 547 F g^{-1}.

A R T I C L E I N F O

Article history:
Received 11 June 2012
Received in revised form
28 September 2012
Accepted 30 September 2012
Available online 9 October 2012

Keywords:
Supercapacitors
XPS
TGA
Raman
FTIR

A B S T R A C T

The composite material was obtained by the polymerization of aniline in the presence of graphene oxide nanosheets. The resulting composite containing polyaniline (72%) and graphene oxide nanosheets (28%) was investigated by XPS, TGA, Raman and IR spectroscopy. A partial reduction of graphene oxide was observed in the process of polymerization. The specific capacitance of the polyaniline/graphene oxide composite electrode in H_2SO_4 (1 M concentration), corresponding to its discharge from 0.700 to 0.052 V, was found to be 547 F g^{-1}.

1. Introduction

The number of publications concerning the study of different materials used as new electrodes for supercapacitors has been growing rapidly. Recently discovered carbon nanostructures provide high specific surface area and high conductivity and could improve the performance of these devices.

Carbon nanomaterials show good mechanical properties. Manifold charge–discharge cycles do not affect their specific capacity, which is not high enough, unfortunately [1]. On the contrary, conducting polymers are characterized by high specific capacity but are unstable under cycling. Among the conducting polymers, inexpensive polyaniline (PANi) shows high conductivity and can be easily synthesized. Composites of PANi with carbon nanomaterials show the best of the intrinsic characteristics of each of the components. For example, the PANi composite with carbon nanofibers shows a specific capacitance (SC) equal to 264 F g^{-1} [2]. The value of SC for single-walled carbon nanotubes is 350–485 F g^{-1} [3–5], and that of multi-walled carbon nanotubes is 322–606 F g^{-1} [6,7]. For the composite of PANi with graphene oxide or with reduced graphene oxide, the situation is much more favorable and the value of SC according to the literature data is in the range from 210 to 1130 F g^{-1} [8–20].

In this work we have studied the chemical composition and structure of the composite material obtained by polymerization of aniline in the presence of graphene oxide nanosheets (GONS). The specific capacity of this composite material is equal to 547 F g^{-1}. This value is in the range of specific capacities published in the

* Corresponding author. Tel./fax: +7 4965223670.
E-mail addresses: shulga@icp.ac.ru, yshulga@gmail.com (Y.M. Shulga).

0378-7753/$ – see front matter
http://dx.doi.org/10.1016/j.jpowsour.2012.09.105

literature for similar materials. However, the value is higher than those of PANi (115 F g^{-1}) and GONS (183 F g^{-1}) [12]. GONS used in the composite material were not reduced previously since it was supposed that GONS would be reduced directly during polymerization [12]. The main goal of our research was to study the interaction of the components in the composite material and to understand the reason of the high dispersion of the SC values for different PANi–GONS composites.

2. Experimental

2.1. Synthesis of graphite oxide

Graphite oxide was synthesized by a modified Hammer's method as described in Ref. [21]. To prepare an aqueous suspension of graphene oxide nanosheets, 300 mg of graphite oxide was mixed with 400 ml of distilled water and the mixture was treated in an ultrasonic bath for 1 h. The resulting suspension was centrifuged for 15 min at 3000 *g* to remove large particles. The elemental composition of GONS after drying at 60 °C was: C (52.99), O (45.4) and H (1.68) (wt. %). According to the Fischer method of water analysis, the composition of GONS was $C_6O_{3.45}H_{1.35}(H_2O)_{0.44}$.

2.2. Synthesis of PANi and PANi–GONS composite material

Aniline sulfate (1.07 g) was dissolved in 50 ml of distilled water. The suspension of GONS was added to the solution with stirring. Concentrated sulfuric acid was added in the reactor to reach the value of pH = 2. The mixture was cooled down to -2 ± 2 °C in an ice bath. Then, 50 ml of aqueous solution of ammonium persulfate was slowly added dropwise to the mixture. The reaction proceeded for 4 h at the above temperature range. The resulting precipitate was centrifuged and repeatedly washed with distilled water to form a dark green pasty mass. The samples for electrochemical studies were prepared by deposition of this dark green substance on a glassy carbon plate of 0.5 × 0.5 × 4 cm in size, followed by drying in air at 60–70 °C. According to elemental analysis, the dried composite material contained: C (55.69), O (28.03), N (7.92), S (4.39) and H (4.04), in wt.%. The content of graphene oxide in composite **1** was 26.5 ± 1.5 wt.%.

The PANi itself was synthesized using a similar procedure but without adding the suspension of GONS to the reaction mixture. According to the chemical analysis, PANi contained: C (53.4), O (24.85), N (10.2), S (6.8) and H (4.88), in wt.%, and the general formula (without the balance of hydrogen) was $C_6N_{0.98}(H_2O)_{0.95}(H_2SO_4)_{0.29}$.

Composite **2** was prepared by mixing the solution of PANi in formic acid and aqueous suspension of GONS. Polyaniline was obtained in the form of the salt of sulfuric acid and was reduced to the base state by treatment with aqueous solution of ammonia for 24 h. After washing in water PANi was dried in air-at 70 °C for 24 h. The 700 mg of PANi in base state was dissolved in 100 ml of concentrated formic acid. The suspension of GONS (250 mg/300 ml water) was slowly added to PANi's water solution. The sediment formed after mixing was repeatedly washed and neutralized with aqueous ammonia. The composite was doped by keeping it in 0.5 M H_2SO_4 during the day. As a result of dopping the composite **2** has changed the color to bright green. The concentration (w/w) of graphene oxide in the final composite **2** was 25%.

X-ray photoelectron spectra (XPS) were measured in a Thermo Scientific K-Alpha spectrometer using monochromatic Al Kα radiation. The working pressure in the chamber of the spectrometer did not exceed 4×10^{-10} Torr. The pass energy (50 eV) was constant in all experiments. The atomic concentrations in the surface layer were calculated from integrated intensities of the peaks, taking into account the literature data for the ionization cross sections [22].

Raman spectra were excited using a laser radiation with the wavelength $\lambda = 633$ nm. The spectra were recorded using LabRAM HR systems. TGA analysis was performed in a Netzsch STA-409 instrument in the temperature range 20–800 °C at the heating rate of 10 deg min^{-1}. Cyclic voltammetry (CV) and charge/discharge characteristics were measured in an electrochemical glass cell using 1 M H_2SO_4 at room temperature in air. Working and auxiliary electrodes were separated by a porous glass membrane. Glassy carbon plate, 1 × 4 cm in size, was used as an auxiliary electrode and an Ag/AgCl electrode was used as a reference electrode. The measurements of electrode potentials relative to the reference electrode were performed with an Elins PS-7 potentiometer.

3. Results and discussion

Raman spectra of the polymer and the composite material are shown in Fig. 1. The attributions of the peaks in the Raman spectrum of polyaniline can be found, for example, in Ref. [23–30]. It should be noted that the peaks at 1620 and 1585 cm^{-1} indicate the presence of benzoid and quinoid rings, respectively, in the investigated polymer. There are also peaks in the spectrum attributed to the sulfate groups (marked as ν) [31–33]. The positions of the peaks attributed to the sulfate groups are the same for the pure polymer and the composite. The presence of benzoid and quinoid rings in the spectrum of the composite cannot be determined because of the overlapping with a more intense G band (1593 cm^{-1}) from graphene oxide. However, almost complete coincidence of the bands in the low-frequency parts of the spectra of the samples being compared leads to the assumption that the structure of the polymer in the composite is similar to that of the pure polymer. It should be noted that in both spectra there is no band at 1678 cm^{-1}, a characteristic of partially degraded polyaniline [34].

The presence of graphene oxide in the composite material is confirmed by the detection of D and G bands in the spectra. The positions of these bands for the composite material (1335 and 1593 cm^{-1}, respectively) are different from those in the original graphene oxide (1374 and 1611 cm^{-1}, respectively). This difference could be the result of chemical interaction of GONS with the polymer. On the other hand, we do not see any shifts of the polymer bands in the composite material in comparison with the pure

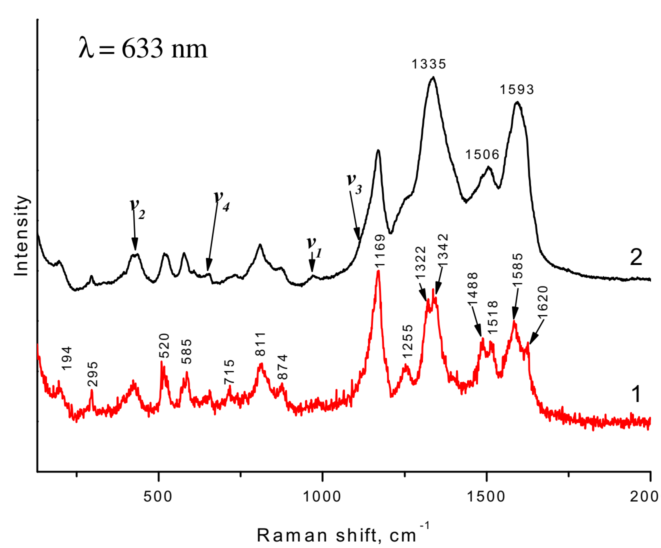

Fig. 1. Raman spectra of the polymer (1) and the composite material (2).

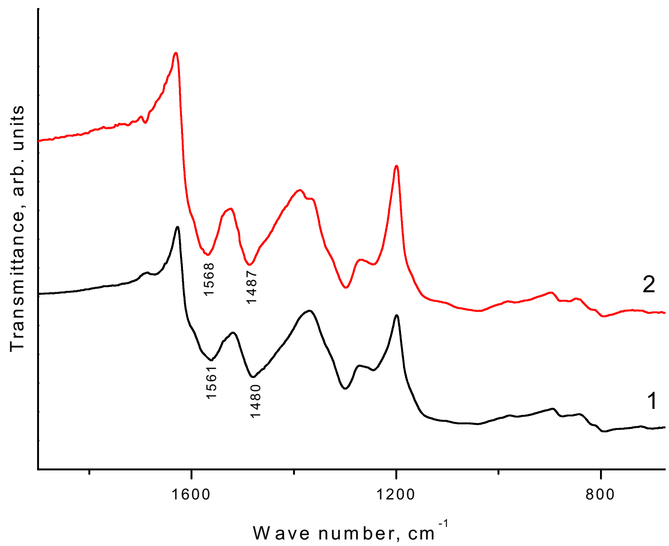

Fig. 2. IR spectra of PANi (1) and PANi–GONS composite (2).

Table 1
The relative concentrations of the elements (in atomic units).

Sample	Method	N/C	O/C	S/C
PANi	Vol.	0.16	0.35	0.05
PANi	Surf.	0.11	0.20	0.16
PANi/GONS	Vol.	0.12	0.38	0.03
PANi/GONS	Surf.	0.08	0.18	0.06

polymer. A possible explanation for this is the small amount of GONS in comparison with the polymer content. Also, we cannot exclude the influence of the superposition of GONS and PANi spectra on the shift of some peaks.

In contrast to the Raman spectra, it is difficult to detect GONS in the IR spectra (Fig. 2) of the nanocomposite. However, the presence of quinoid and benzoid rings in the composite is confirmed by detecting absorption bands at 1568 and 1488 cm^{-1}, respectively, in the IR spectra [34]. Moreover, from comparison of these bands in the spectra of pure PANi and those for the composite, one can conclude that quinoid structures increase in the composite in comparison with pure PANi. It should also be noticed that intercalation of PANi by GONS is accompanied by a 7–8 cm^{-1} shift in the absorption bands to higher wavelength numbers.

The surface concentrations of the elements calculated from X-ray photoelectron spectroscopy can be compared with those determined from the elemental analysis. Table 1 shows that surface concentrations are significantly different from bulk concentrations for sulfur only. This is consistent with the idea that the $[SO_4]^{2-}$ groups are located mainly on the border of the polymer globules.

Fig. 3 shows the C1s photoelectron spectrum of polyaniline, showing a single asymmetric peak. A similar C1s peak was observed for polyaniline in other publications [35–37]. The shoulder on the side of higher binding energy can be explained by the presence of carbon atoms with an excessive charge, greater than that of carbon atoms bounded by hydrogen and carbon atoms only. Such carbon atoms are known to exist in polyaniline and are bonded with nitrogen atoms. In addition, the charge located on the nitrogen atom can vary, depending on the degree of reduction of the polymer. Thus, to a first approximation the deconvolution of the spectrum may be done with only two components. However, the actual number of components must be larger, if we take into account the fact that the charge located on the nitrogen atom is different for the imine and amine groups.

Fig. 3A shows the deconvolution of the XPS spectrum into two Gaussian curves, in which all adjustable parameters (binding energy, intensity and full width at half maximum (FWHM)) were used for verification. It is clear that the description of the XPS spectrum by two Gaussian curves is not sufficient since the high-energy part of the spectrum is not described adequately. The description of the spectrum with three Gaussian curves (Fig. 3B) seems to be more adequate. However, there is no reasonable explanation for the higher value of FWHM for the peaks attributed to carbon atoms bonded with nitrogen in comparison with FWHM of the main XPS peak attributed to non-charged carbon atoms. Moreover, the intensity of the peaks corresponding to carbon atoms bonded to nitrogen atoms is noticeably higher than 33%, while the percentage of these atoms in the polymer, according to the stoichiometric ratio, should be exactly equal to 33%.

The description of the spectrum by three Gaussian curves with FWHMs equal to the FWHM value of the main peak, for which its determination had sufficient accuracy, is not also completely adequate.

Some authors used more than three Gaussian curves to describe the C1s peak for polyaniline and obtained a good fitting [35,37]. The peak with E_b = 288.3 eV was attributed to carbon atoms bonded with oxygen atoms [36] and this assumed partial degradation of polyaniline as a result of oxidation. According to the Raman spectra, there are no C–O groups in our structure. We suppose that the long tail at higher binding energies of the main C1s peak of polyaniline is associated with high conductivity rather than with the presence of positively charged carbon atoms. In other words, asymmetry of the C1s peak for polyaniline could be partly due to excitation of

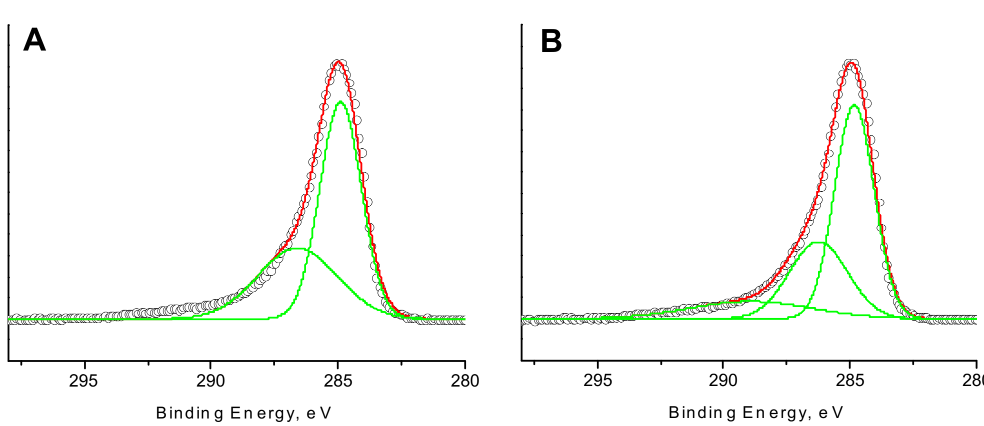

Fig. 3. C1s XPS core-level spectra (open circles) and deconvolution by 2 (A) and 3 (B) Gaussian components.

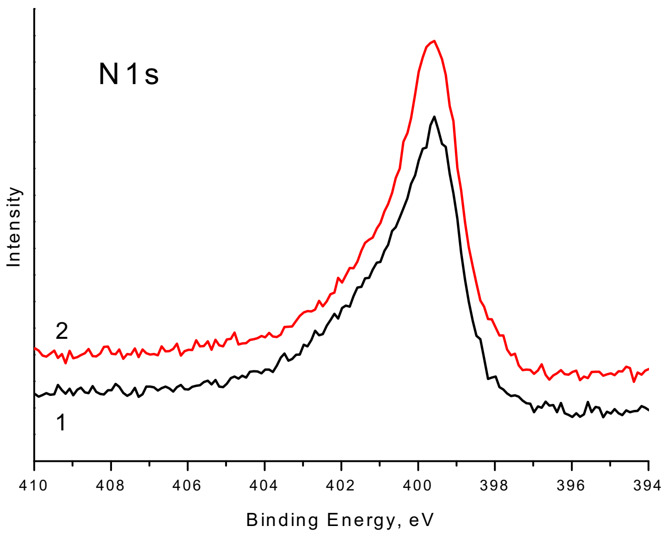

Fig. 4. N1s XPS core-level spectra of polyaniline (1) and PANi–GONS composite (2).

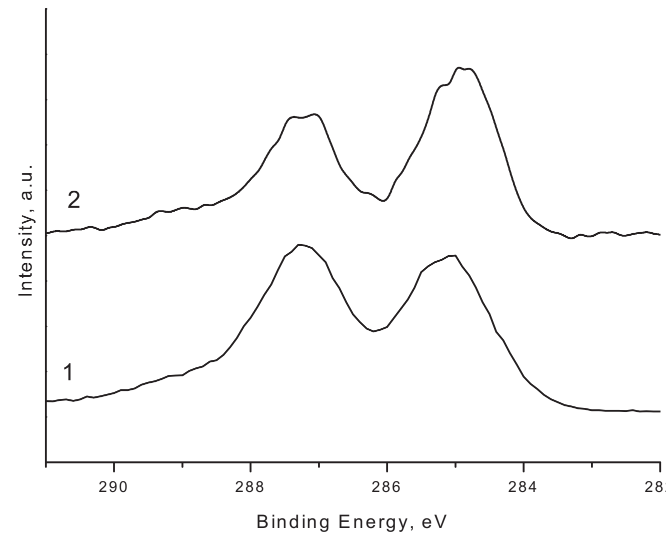

Fig. 6. C1s XPS core-level spectra of initial GONS (1) and GONS in the composite (2).

electron–hole pairs, as observed in metals [38]. A noticeable contribution to the asymmetry of the C1s peak can also be due to the energy losses accompanying photoionization and associated with excitation of interband transitions and plasma oscillations of π-electrons [39].

The N1s photoelectron peak of our polymer appears as an asymmetric peak with the maximum at 399.6 eV (Fig. 4). It is known that nitrogen in polyaniline can be present as imine (–N=), amine (–NH–) and the corresponding protonated forms, if protonation is possible. The last form can be generated as a result of internal oxidation and/or protonation. Here, it is assumed that imine and amine are detected in the photoelectron spectra as peaks with maxima at 398.2 and 399.4 eV, respectively [35–37,40–44]. Unfortunately, there is no data concerning the peaks corresponding to positively charged nitrogen atoms in the photoelectron spectra of PANi. Obviously, such peaks should be found in the XPS spectra at energies $E_b > 400$ eV.

The shape analysis of the N1s peak has shown no nitrogen of the imine type in the polymer. The main nitrogen group is –NH– (more than 60%). Positively charged nitrogen atoms are also present in the sample. The fraction of these atoms (or the doping degree of the polymer) is less than 40%. A more precise estimation cannot be done since the spectrum deconvolution does not take into account the reasons discussed regarding the deconvolution of the C1s peak. The N1s spectrum of the composite is the same as that of the polymer (see Fig. 4). Therefore, the nitrogen atoms are present in our structure in two groups, namely, amine (–NH–) and cations (N+).

The inset on Fig. 5, comparing the C1s peaks in pure polyaniline and in the composite, shows the difference spectrum obtained by subtraction, as described in Ref. [45]. The difference spectrum corresponds to the C1s spectrum of graphene oxide nanosheets present in the composite and is well approximated by three Gaussian curves. According to Ref. [46–51], a peak with $E_b = 284.9$ eV is due to the carbon atoms closely surrounded by other carbon atoms only. The second peak (287.2 eV) is attributed to carbon atoms bonded with one oxygen atom, i.e., epoxy (>COC<) and/or hydroxyl (>C–OH) groups. The third peak can be attributed to carboxyl (–COOH) groups, i.e., carbon atoms double bonded with oxygen atoms. Comparing the intensities of individual peaks, one can conclude that 37% of the carbon atoms of graphene oxide nanosheets are bonded with one oxygen atom, and 15% are double bonded with oxygen in the composite.

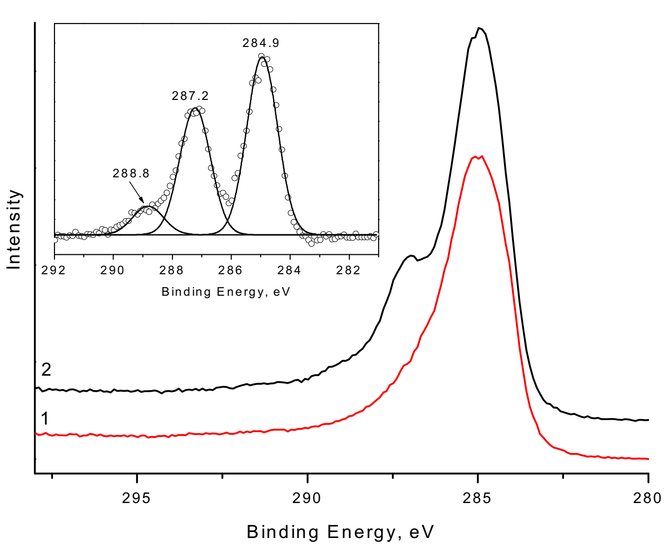

Fig. 5. C1s XPS core-level spectra of polyaniline (1) and PANi–GONS composite (2). Intensities of the spectra are calibrated on the intensity of the N1s peak. The inset shows the spectrum obtained by subtracting spectrum 1 from spectrum 2.

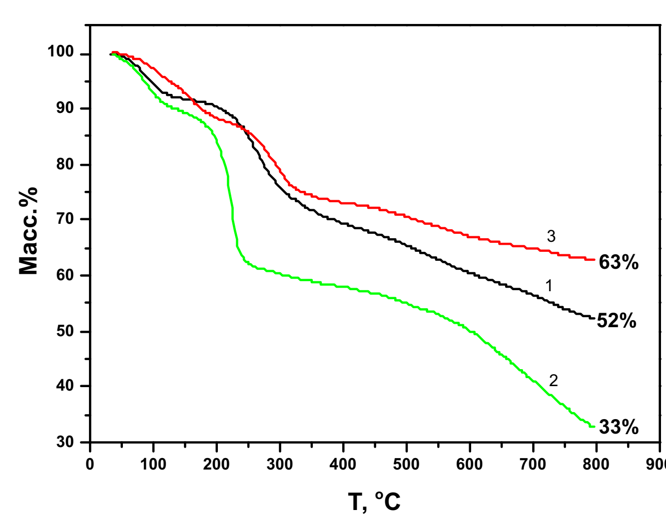

Fig. 7. TG curves for PANi (1), GONS (2) and composite PANi–GONS (3).

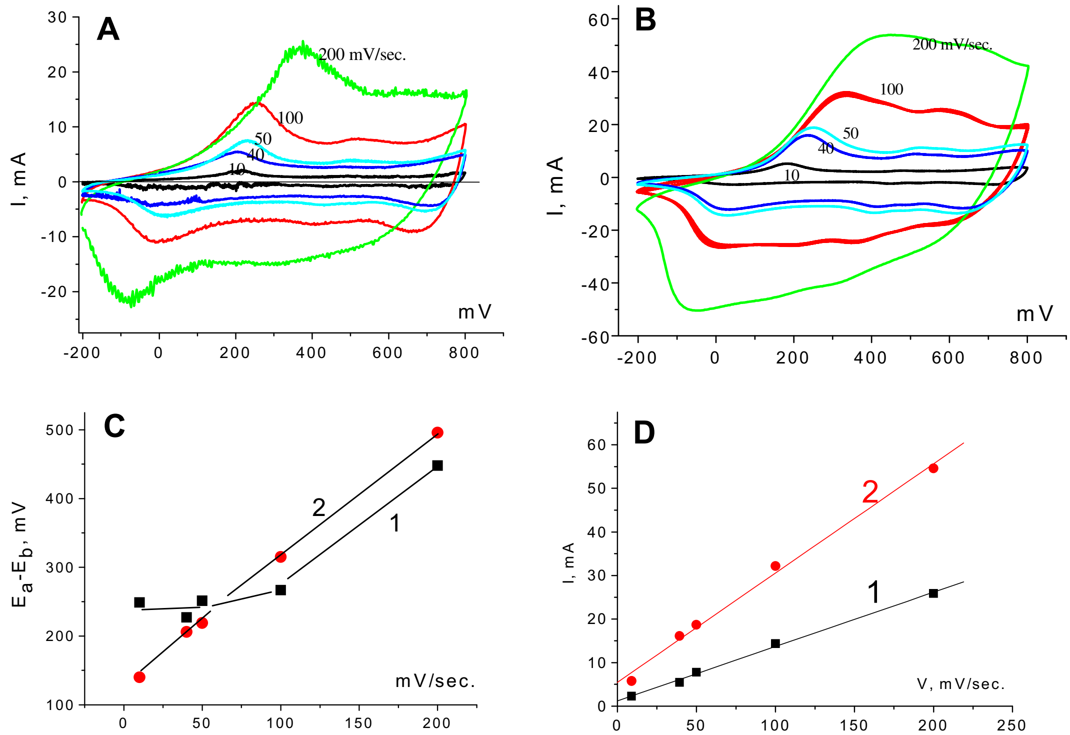

Fig. 8. CVA for composite **1** with loading 0.00021 g (A) and for composite **2** with loading 0.00031 g (B) in 1 M H_2SO_4 at speeds of cycling 10, 40, 50,100, 200 mV s^{-1}. (C) – The dependence of ΔE on the rate of cycling of the composite **1** (curve 1) and composite **2** (curve 2); (D) dependence of anodic current on the sweep rate for a composite **1** (curve 1) and composite **2** (curve 2). Ma.

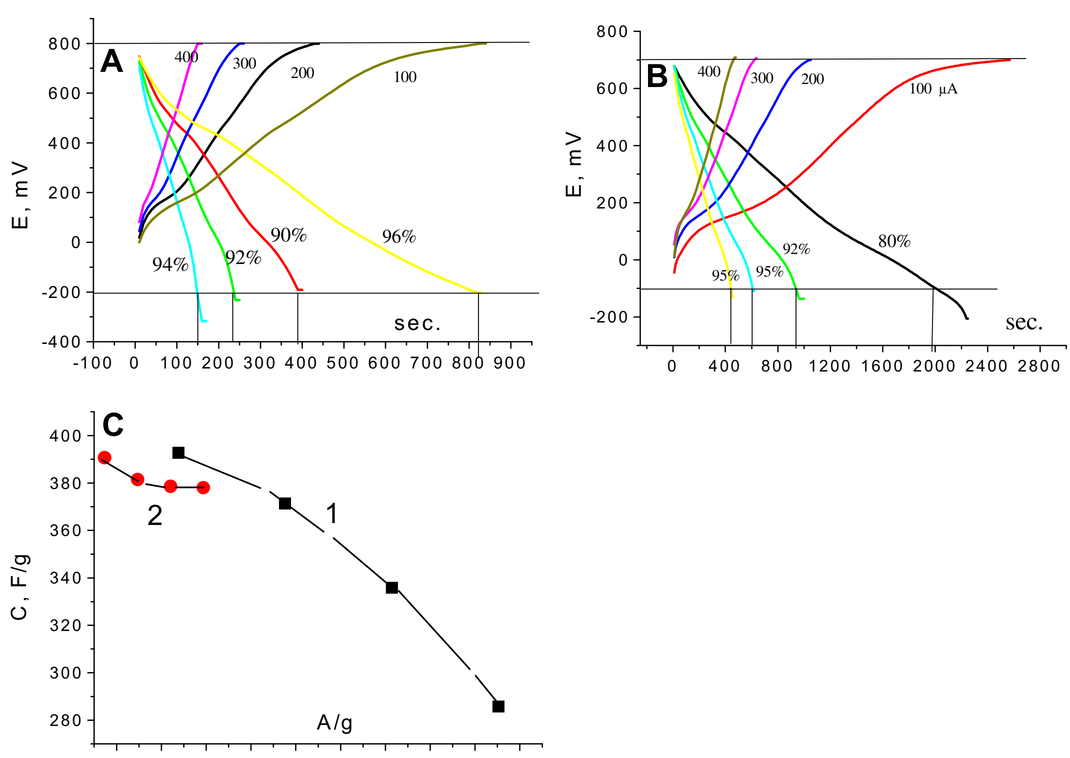

Fig. 9. Charge–discharge curves for composite **1** (A) and composite **2** (B). (C) – The specific capacitance of composites as a function of current magnitude for a composite **1** (curve 1) and composite **2** (curve 2). The percentages on the figure are corresponding to the Coulombic efficiencies of the charge/discharge processes.

The C1s peak of the initial GO nanosheets differs from that of the composite (Fig. 6). According to the deconvolution procedure, the intensities of the second and third peaks amount to 46 and 9% of the total intensity. Thus, GONS were partially reduced in the process of polymerization. This effect was reported earlier in Ref. [12]. But in our case, the number of carbon atoms in GONS bonded with oxygen is higher than that in the composite studied in Ref. [12]. This may be due to either different polymerization conditions or different methods of determining the reduction degree.

Three stages are usually distinguished on a thermogravimetric (TG) curve of polyaniline (see, for example [52]). At the first stage (from room temperature up to 100 °C), weight loss is associated with the loss of water vapor absorbed in the sample in contact with air (Fig. 7). The second stage (200–320 °C) is attributed to a decomposition of sulfuric acid or sulfate ions. The polyaniline is degraded at $T > 360$ °C.

Three stages can also be distinguished on the TGA curve for GONS. The reason for the weight loss for GONS at $T < 100$ °C is the same as for polyaniline. The second well-pronounced stage at 180–240 °C is associated with the release of water molecules formed as a result of the reaction between two hydroxyl groups. Carbon oxides are also formed at this stage, as well as at higher temperatures [53], although at a reduced reaction rate, since to form a CO_2 molecule we need two oxygen containing groups, the number of which is gradually decreasing. It should be noticed that the thermal stability of the GONS is lower than that of polyaniline. The residual weight is 33% in GONS and 52% in polyaniline at 800 °C. Fig. 7 shows that the thermal stability of the composite is significantly higher than that of the initial components. This may be due to the reduction of GONS in the polymerization reaction and the difference in globular structure between the pure polymer and the polymer in the composite.

Fig. 8a and b show the cyclic voltammetry of freshly prepared composite **1** and composite **2**. Fig. 8c shows the peak potential separation ΔE_p ($\Delta E_p = E_{pc} - E_{pa}$, here E_{pc} and E_{pa} are potentials of cathode and anode peaks) with increasing ν. From this graph it is clear that ΔE_p generally increases with ν for both composites. But for composite **1**, ΔE_p does not change practically at $0 < \nu < 100$ mV s^{-1}. The deterioration of reversibility for composite **1** starts at $\nu > 100$ mV s^{-1}.

For composite **2**, ΔE_p lineally grows with ν, which means that any increase in scan rate causes deterioration of the cycling reversibility of redox processes in the composite. This behavior is probably due to ohmic losses. This conclusion follows from the graph of the dependence of anodic current on the rate of cycling, which shows a linear relationship (Fig. 8d). In the case of diffusion restrictions, a linear dependence on the square root of the scan rate should be observed.

Fig. 9 shows the charge–discharge curves of both composites in the current range from 100 to 400 μA, while the current densities are in the range of 0.1–2 A g^{-1}. From these discharge curves, specific capacities were calculated for both composites using the formula: $C = It/P\Delta E$, where I is discharge current, t is time of discharge, P is weight of the sample, ΔE is range potential. The results of these calculations are shown in Fig. 9c. These graphs show that composite **2** behaves in a much more stable way.

Thus, the specific capacity of the freshly prepared PANi–GONS composite is not high. In order to increase the specific capacity, we have developed a special procedure: the small negative potential (−0.35 V) was applied to the electrode for 10–20 s. After such treatment, CV exhibits redox current peaks which indicate the electroactivity of polyaniline (Fig. 10, inset). On the discharge curve (Fig. 10) it is seen that the electrode works as a capacitor (fast stage) and as an electrochemical battery (slow stage). The slow stage of the discharge is caused by oxidation of polyaniline. The assessment of the capacity of such electrode with the simplified formula $C = It/P\Delta E$ is not possible because of the existence of a slow stage.

The results of the numerical calculations of $dE/dt = I/C$ are shown in Fig. 11. The specific capacity for the rapidly decaying part of the curve is 547 F g^{-1}. However, if the calculations include the

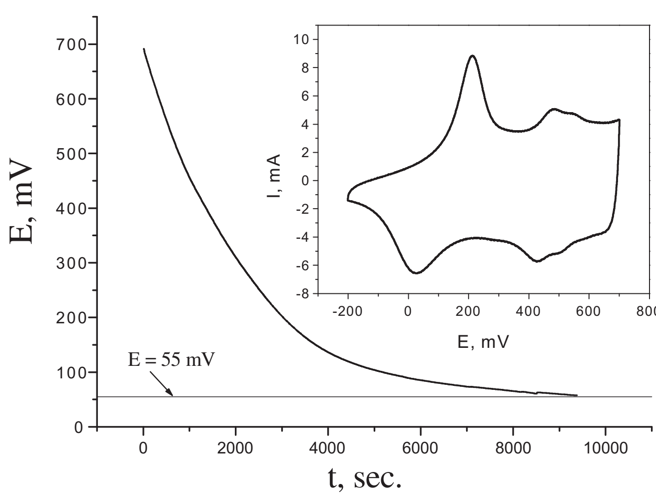

Fig. 10. The discharge curve ($i = 0.01$ mA) in 1 M H_2SO_4 for the PANi–GONS electrode (with loading 0.28 mg) after special treatment (see the text). The inset shows a typical CVA curve for this electrode (the sweep rate is 50 mV s^{-1}).

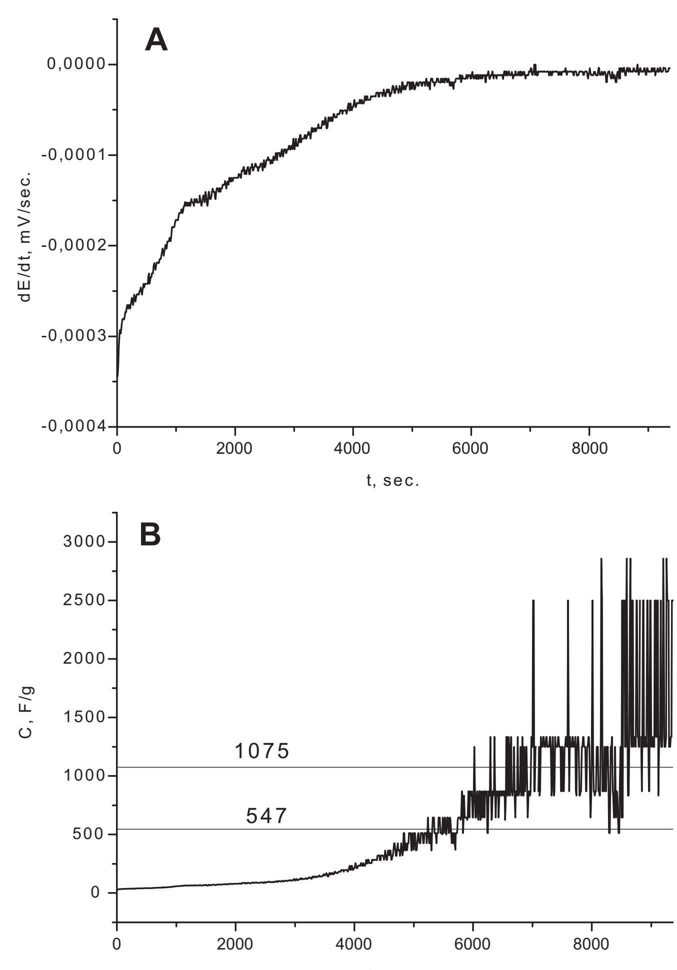

Fig. 11. Dependences of dE/dt (A) and C (B) on time.

shallow part of the curve, then, as we see on the graph, the specific capacity is well above 1000 F g^{-1}. We emphasize that we were not able to convert composite **2** into a state of high specific capacity.

4. Conclusions

The detailed study of the composite material prepared by the synthesis of polyaniline in the presence of GONS shows that a polymer matrix interacts with graphene oxide in the process of polymerization. As a result, graphene oxide is reduced partially in spite of the presence of other oxidants in the reaction mixture. One can suppose that partially reduced graphene oxide provides higher conductivity to the composite as compared with polyaniline.

The specific capacitance of the PANi–GONS electrode (composite **1**) in H_2SO_4 (1 M concentration), corresponding to its discharge from 0.700 to 0.052 V, was found to be 547 F g^{-1} ($I_d = 0.01$ mA, $t_d = 5500$ s). A value greater than 1000 F g^{-1} for the specific capacity could be obtained if the calculation of capacitance included a flat segment of the discharge curve ($I_d = 0.01$ mA, $t_d > 7000$ s).

From the present results, it is shown that the specific capacity of the system is strongly affected by the method of composite production and the preliminary electrochemical treatments. For a more reliable assessment of the supercapacitor based on the PANi–GONS system one must specify also the conditions under which this value was obtained (discharge current and discharge time).

Acknowledgments

The work is partially supported by Russian Foundation for Basic Research (Project 12-03-00261-a).

References

[1] W.C. Chen, T.C. Wen, H.S. Teng, Electrochim. Acta 48 (2003) 641.
[2] J. Zhang, L.-B. Kong, B. Wang, Y.-C. Luo, L. Kang, Synth. Met 159 (2009) 260.
[3] M. Cochet, G. Louarn, S. Quillard, J.P. Buisson, S. Lefrant, J. Raman Spectrosc. 31 (2000) 1041.
[4] X.S. Du, M. Xiao, Y.Z. Meng, Eur. Polym. J. 40 (2004) 1489.
[5] S.R. Sivakkumar, W.J. Kim, J.-A. Choi, D.R. MacFarlane, M. Forsyth, D.-W. Kim, J. Power Sources 171 (2007) 1062.
[6] Y. Sun, S.R. Wilson, D.I. Schuster, J. Am. Chem. Soc. 123 (2001) 5348.
[7] Y.-G. Wang, H.-Q. Li, Y.-Y. Xia, Adv. Mater. 18 (2006) 2619.
[8] D.-W. Wang, F. Li, J. Zhao, W. Ren, Z.-G. Chen, J. Tan, Z.-S. Wu, I. Gentle, G.Q. Lu, H.-M. Cheng, ACS Nano 3 (2009) 1745.
[9] H. Wang, Q. Hao, X. Yang, L. Lu, X. Wang, ACS Appl. Mater. Interfaces 2 (2010) 821.
[10] Q. Wu, Y. Xu, Z. Yao, A. Liu, G. Shi, ACS Appl. Mater. Interfaces 4 (2010) 1963.
[11] J. Xu, K. Wang, S.-Z. Zu, B.-H. Han, Z. Wei, ACS Appl. Mater. Interfaces 4 (2010) 5019.
[12] J. Yan, T. Wei, B. Shao, Z. Fan, W. Qian, M. Zhang, F. Wei, Carbon 48 (2010) 487.
[13] L. Mao, K. Zhang, H.S.O. Chan, J.S. Wu, J. Mater. Chem. 22 (2012) 80.
[14] J. Li, H.Q. Xie, Y. Li, J. Liu, Z.X. Li, J. Power Sources 196 (2011) 10775.
[15] X.J. Lu, H. Dou, S.D. Yang, L. Hao, L.J. Zhang, L.F. Shen, F. Zhang, X.G. Zhang, Electrochim. Acta 56 (2011) 9224.
[16] H.L. Wang, Q.L. Hao, X.J. Yang, L.D. Lu, X. Wang, Nanoscale 2 (2010) 2164.
[17] K. Zhang, L.L. Zhang, X.S. Zhao, J.S. Wu, Chem. Mater. 22 (2010) 1392.
[18] J. Yan, T. Wei, Z.J. Fan, W.Z. Qian, M.L. Zhang, X.D. Shen, F. Wei, J. Power Sources 195 (2010) 3041.
[19] S. Liu, X.H. Liu, Z.P. Li, S.R. Yang, J.Q. Wang, New J. Chem. 35 (2011) 369.
[20] H. Gomez, M.K. Ram, F. Alvi, P. Villalba, E. Stefanakos, A. Kumar, J. Power Sources 196 (2011) 4102.
[21] V.E. Muradian, M.G. Ezernitskaya, V.I. Smirnova, N.M. Kabaeva, M.E. Volpin, J. Gen. Chem. 61 (1991) 2626 (in Russian).
[22] C.D. Wagner, W.M. Riggs, L.E. Davis, J.F. Moulder, G.E. Muilenberg (Eds.), Handbook of X-Ray Photoelectron Spectroscopy, Eden Prairie, Minnesota, 1979.
[23] Y. Furukawa, F. Ueda, Y. Hyodo, I. Harada, T. Nakajima, T. Kawagoe, Macromolecules 21 (1988) 1297.
[24] M. Lapkowski, K. Berrada, S. Quillard, J.G. Louarn, S. Lefrant, A. Prod, Macromolecules 28 (1995) 1233.
[25] S. Quillard, G. Louarn, J.P. Buisson, S. Lefrant, J. Masters, A.G. MacDiarmid, Synth. Met (1992) 525. 49–50.
[26] S. Quillard, G. Louarn, S. Lefrant, A.G. MacDiarmid, Phys. Rev. B 50 (1994) 12496.
[27] G. Louarn, M. Lapkoaski, S. Quillard, A. Pron, J.P. Buisson, S.J. Lefrant, Phys. Chem. 100 (1996) 6998.
[28] M. Bernard, A.H. Goff, Synth. Met 85 (1997) 1145.
[29] L.D. Arsov, W. Plieth, G. Koûmehl, J. Solid State Electrochem. 2 (1998) 355.
[30] Lijuan Zhang, Meixiang Wan, J. Phys. Chem. B 107 (2003) 6748.
[31] R. Fehrmann, B. Krebs, G.N. Papatheodorou, R.W. Berg, N.J. Bjerrum, Inorg. Chem. 25 (1986) 1571.
[32] R.L. Frost, M.L. Weier, W. Martens, J. Raman Spectrosc. 36 (2005) 435. 4.
[33] R.L. Frost, W.N. Martens, A.J. Locke, J. Raman Spectrosc. 38 (2007) 1429.
[34] S.-A. Chen, H.-T. Lee, Macromolecules 28 (1995) 2858.
[35] H.S.O. Chan, S.C. Ng, W.S. Sim, K.L. Tan, B.T.G. Tan, Macromolecules 25 (1992) 6029.
[36] C. Barthet, S.P. Armes, M.M. Chehimi, C. Bilem, M. Omastova, Langmuir 14 (1998) 5032.
[37] Y. Chen, E.T. Kang, K.G. Neoh, S.L. Lim, Z.H. Ma, K.L. Tan, Colloid Polym. Sci. 279 (2001) 73.
[38] P.W. Anderson, Phys. Rev. Lett. 18 (1967) 1049.
[39] Y.M. Shulga, V.I. Rubtsov, A.S. Lobach, Z. Phys. B 93 (1994) 327.
[40] Z.F. Li, M.T. Swihart, E. Ruckenstein, Langmuir 20 (2004) 1963.
[41] H. Zhang, H.X. Li, H.M. Cheng, J. Phys. Chem. B 110 (2006) 9095.
[42] B.C. Beard, P. Spellane, Chem. Mater. 9 (1997) 1949.
[43] S.-A. Chen, L.C. Lin, Macromolecules 28 (1996) 1239.
[44] K.L. Tan, B.T.G. Tan, E.T. Kang, K.G. Neoh, Phys. Rev. B 39 (1989) 8070.
[45] Y.M. Shulga, S.A. Baskakov, V.V. Abalyaeva, O.N. Efimov, N.Y. Shulga, A. Michtchenko, L. Lartundo-Rojas, L.A. Moreno-Rojas, J.G. Cabañas-Moreno, Proceeding Int. Conf. Nanomaterials: Application and Properties 1, 2012, 04NEA01(2pp).
[46] T. Szabo, O. Berkesi, P. Forgo, K. Josepovits, Y. Sanakis, D. Petridis, I. Dekany, Chem. Mater. 18 (2006) 2740.
[47] J.R. Lomeda, C.D. Doyle, D.V. Kosynkin, W.-F. Hwang, J.M. Tour, J. Am. Chem. Soc. 130 (2008) 16201.
[48] C. Xu, X. Wang, J. Zhu, J. Phys. Chem. C 112 (2008) 19841.
[49] S. Park, K.-S. Lee, G. Bozoklu, W. Cai, S.B.T. Nguyen, R.S. Ruoff, ACS Nano 2 (2008) 572.
[50] J.I. Paredes, S. Villar-Rodil, P. Solis-Fernandez, A. Martinez-Alonso, J.M.D. Tascon, Langmuir 25 (2009) 5957.
[51] C. Shan, H. Yang, J. Song, D. Han, A. Ivaska, L. Niu, Anal. Chem. 81 (2009) 2378.
[52] N.T. Tung, T.V. Khai, M. Jeon, Y.J. Lee, H. Chung, J.-H. Bang, D. Sohn, Macromol. Res. 19 (2011) 203.
[53] Y.M. Shulga, V.M. Martynenko, V.E. Muradyan, S.A. Baskakov, V.A. Smirnov, G.L. Gutsev, Chem. Phys. Lett. 498 (2010) 287.